Excitability and optical pulse generation in semiconductor lasers driven by resonant tunneling diode photo-detectors

Bruno Romeira,[1,*] Julien Javaloyes,[2] Charles N. Ironside,[3] José M. L. Figueiredo,[1] Salvador Balle,[2] and Oreste Piro[2]

[1]*Centro de Electrónica, Optoelectrónica e Telecomunicacões (CEOT), Departamento de Física, Universidade do Algarve, Campus de Gambelas, 8005-139 Faro, Portugal*
[2]*Departament de Física, Universitat de les Illes Balears, C/ Valldemossa km.7'5, E-07122, Palma de Mallorca, Spain*
[3]*School of Engineering, University of Glasgow, Glasgow G12 8QQ, UK*
[*]*bmromeira@ualg.pt*

Abstract: We demonstrate, experimentally and theoretically, excitable nanosecond optical pulses in optoelectronic integrated circuits operating at telecommunication wavelengths (1550 nm) comprising a nanoscale double barrier quantum well resonant tunneling diode (RTD) photo-detector driving a laser diode (LD). When perturbed either electrically or optically by an input signal above a certain threshold, the optoelectronic circuit generates short electrical and optical excitable pulses mimicking the spiking behavior of biological neurons. Interestingly, the asymmetric nonlinear characteristic of the RTD-LD allows for two different regimes where one obtain either single pulses or a burst of multiple pulses. The high-speed excitable response capabilities are promising for neurally inspired information applications in photonics.

OCIS codes: (250.3140) Integrated optoelectronic circuits; (250.5590) Quantum-well, -wire and -dot devices; (250.5960) Semiconductor lasers; (040.5160) Photodetectors.

References and links

1. A. L. Hodgkin and A. F. Huxley, "A quantitative description of membrane current and its application to conduction and excitation in nerve," J. Physiol.-London **117**(4), 500–544 (1952).
2. L. Kuhnert, K. I. Agladze, and V. I. Krinsky, " Image processing using light-sensitive chemical waves," Nature **337**, 244–247 (1989).
3. F. Pedaci, Z. Huang, M. V. Oene, and N. H. Dekkery, " Excitable particles in an optical torque wrench," Nat. Phys. **7**, 259–264 (2011).
4. S. Barbay, R. Kuszelewicz, and A. M. Yacomotti, "Excitability in a semiconductor laser with saturable absorber," Opt. Lett. **36**(23), 4476–4478 (2011).
5. D. Goulding, S.P. Hegarty, O. Rasskazov, S. Melnik, M. Hartnett, G. Greene, J. G. McInerney, D. Rachinskii, and G. Huyet, " Excitability in a quantum dot semiconductor laser with optical injection," Phys. Rev. Lett. **98**(15), 153903 (2007).
6. A. S. Samardak, A. Nogaret, N. B. Janson, A. Balanov, I. Farrer, and D. A. Ritchie, " Spiking computation and stochastic amplification in a neuron-like semiconductor microstructure," J. Appl. Phys. **109**(10), 102408 (2011).
7. B. Lindner, J. Garcia-Ojalvo, A. Neiman, and L. Schimansky-Geier, " Effects of noise in excitable systems," Phys. Rep. **392**(6), 321–424 (2004).
8. F. Hartmann, L. Gammaitoni, S. Höfling, A. Forchel, and L. Worschech, "Light-induced stochastic resonance in a nanoscale resonant-tunneling diode," Appl. Phys. Lett. **98**(24), 242109 (2011).
9. P. Mazumder, S.-R. Li, and I.E. Ebong, " Tunneling-based cellular nonlinear network architectures for image processing," IEEE Trans. Very Large Scale Integration (VLSI) Systems **17**(4), 487–495 (2009).

#189632 - $15.00 USD Received 7 May 2013; revised 21 Jun 2013; accepted 2 Jul 2013; published 30 Aug 2013

10. B. Romeira, J. Javaloyes, J.M.L. Figueiredo, C.N. Ironside, H.I. Cantu, and A.E. Kelly, "Delayed feedback dynamics of Lienard-type resonant tunneling-photo-detector optoelectronic oscillators," IEEE J. Quantum Electron. **49**(1), 31–42 (2013).
11. M. R. DeYong, R. L. Findley, and C. Fields, "The design, fabrication, and test of a new vlsi hybrid analog-digital neural processing element," IEEE Trans. Neural Netw. **3**(3), 363–374 (1992).
12. Y. V. Pershin and M. D. Ventra, " Experimental demonstration of associative memory with memristive neural networks," Neural Networks **23**(7), 881–886 (2010).
13. J. N. Schulman, H. J. D. Santos, and D. H. Chow, "Physics-based RTD current-voltage equation," IEEE Electron Dev. Lett. **17**(5), 220–222 (1996).

1. Introduction

Excitability is a concept originally coined to describe the capacity of living organisms (or of their constituent cells) to respond strongly to a relatively weak external stimulus. It has been used to describe wave propagation in muscles and nerves [1], and how excitable pulses, which are almost identical in shape and duration, travel through the cardiac and nervous systems. For stimuli that overcome a threshold, the response consists of a pulse (whose shape depends only on the excitable system at hand but not on the details of the stimulus) followed by a lapse, called the refractory time, during which the system does not respond to stimuli.

The potential of the excitable response for temporal and spatial information processing is huge. The aforementioned excitable response characteristics confer to the data transmission systems based upon this mechanism a high degree of robustness due to their inherent signal reshaping capabilities. In the spatial domain, a photosensitive Belousov-Zhabotinsky reaction was used to perform image processing [2], with capabilities such as smoothing and Sobel filter edge detection. Recently, an optical torque wrench [3] was employed as a sensing technique based in the excitability concept capable of detecting single perturbation events.

In the last decade there has been a quest for electro-optical excitable systems capable of responding on ns or sub-ns time scales. Recently in semiconductor lasers, short pulses (0.73 ns) were obtained in the case of a monolithic vertical cavity laser with intracavity saturable absorber [4]; however, the inter-spike period in [4] was long (250 ns). This may suggest that the lethargic time of this class III excitable system was long although the potential for higher speed, only limited by the carrier lifetime, in principle exists. Another example of generation of fast optical excitable pulses can be found in [5] showing excitability in a quantum dot semiconductor laser with optical injection. In electronic systems, a neuron-like semiconductor microstructure [6] was recently explored but operates only at speed of the order of 20 kHz and do not possess an optical output. Here, we investigate an electrical-optical neuron-like pulsating optoelectronic integrated circuit operating at room temperature and around the 1550 nm telecommunication wavelengths, which contain the fundamental ingredients in order to fulfill the excitability paradigm. Our optoelectronic system possesses the inherent capabilities for being used in the framework of bio-inspired data processing: a high potential for integrability, an intrinsic high speed response and quadruple electronic and optical inputs/outputs. Last but not least, the excitable response consists in an optical and voltage pulse which is not always the case, see e.g. the two-plateaus wave form of the FitzHugh-Nagumo system [7].

The excitable optoelectronic oscillator system, Fig. 1(a), proposed here is formed by a double barrier quantum well (DBQW) resonant tunneling diode (RTD) photo-detector (PD) driving a commercial communications laser diode (LD). The RTD provides a non-monotonic current-voltage (I-V) characteristic with a region of negative differential resistance (NDR), Fig. 1(b), that confers the RTD excitable properties. At the same time, its nanoscale structure allows for extreme compactness and high-speed operation. RTDs have been recently proposed for the study of biological neuron dynamics motivated by the observation of stochastic resonance in a noise-driven low-frequency bistable RTD [8], and for RTD-based cellular neural networks

#189632 - $15.00 USD Received 7 May 2013; revised 21 Jun 2013; accepted 2 Jul 2013; published 30 Aug 2013

(CNN) [9] to perform complex parallel information processing. Here we exploit them only for the generation of ns excitable optical pulses, but the possibility of using RTDs with photo-detection capabilities permits to develop fully opto-electronic excitable systems by reinjecting part of the light emitted by the LD into the RTD by using an optical fiber [10].

To our knowledge, the development of high-speed RTD-based excitable optoelectronic systems in a simple and compact hybrid integrated circuit, sensitively controlled and operating in both the electrical and the optical domains is still a missing piece in the quest of exploiting the full capabilities of spiking neuron-type behavior in future information processing needs. Advances in this regard could take an important step forward in the development of ultra-fast neuro-inspired data processing [2, 11], switching in optical networks, but also neural function emulation like e.g. associative memory networks [12].

2. The excitable optoelectronic oscillator and experimental setup

The excitable optoelectronic oscillator reported here consists of an RTD monolithic integrated within a waveguide photo-detector connected in series with a laser diode in a hybrid optoelectronic integrated circuit, Fig. 1(a). Adding a laser diode does not change the basic shape of the RTD's nonlinear I-V characteristic, it just shifts the peak and valley regions to higher voltages (a shift of around 0.84 V, i.e., the voltage drop across the laser $p-n$ junction) while the current values are left unchanged, Fig. 1(b). Therefore, the nonlinearity of the RTD is preserved in the laser output and the RTD provides a dynamical bias current control for the laser diode conferring to this optoelectronic circuit configuration the necessary conditions to operate as an excitable system with high speed response and quadruple electronic and optical input/output functionalities. Therefore, this setup can be transposed and adapted readily to other types of laser devices and systems like e.g. VCSELs or mode-locked devices.

The RTD devices forming the RTD-LD excitable optoelectronic oscillator consist of a 6 nm wide InGaAs well sandwiched between 2 nm wide AlAs barriers embedded in the core of a unipolar InAlAs/$In_{0.53}Ga_{0.42}Al_{0.05}As$/InP structure on semi-conducting InP substrates. The RTDs fabricated form a ridge waveguide of 4 μm width and 150 μm length, which can be used as photo-detectors around $\lambda = 1550$ nm [10][Fig. 1(a)]. The LD (CST Global Ltd.) consists of an InGaAsP multi-quantum-well active region operating in continuous-wave mode at a center wavelength around 1550 nm, with 6 mA threshold current, Fig. 1(b), and more than 10 mW optical output power. The RTD photo-detector and LD dies are connected in series trough a 50 Ω microstrip transmission line in a printed circuit board [10]. The equivalent electrical circuit schematic of the hybrid integrated RTD-LD circuit is illustrated in Fig. 1(c) showing the RTD capacitance ($C \sim 4.5\,$pF) together with the overall inductance L contribution from the transmission line and bond wires that set the circuit's characteristic operation frequency [10]. The voltage dependent current source $F(V)$ describes the RTD-LD nonlinearity and R accounts for the circuit equivalent resistance. The electrical input of the RTD-LD allows for the bias control, V_{dc}, and application of external electrical signals, V_{in}/V_{noise}, while the electrical output, V, is measured across the RTD-LD.

The experimental setup comprises the driving electrical signals generated by an Agilent 33250A arbitrary waveform generator consisting either of a square or a pulse shape signals, V_{in}, or a Gaussian noise voltage signal, V_{noise}, with 50 MHz bandwidth. The input signal and the d.c. bias voltage, V_{dc}, are added electrically using a bias tee. The electrical voltage output across the RTD-LD is monitored in time domain using a 2 GHz bandwidth oscilloscope and the laser output intensity is monitored by a 50 GHz bandwidth photo-detector with 0.65 A/W responsivity at 1550 nm (u^2t Photonics XPDV2020R) connected to the oscilloscope.

#189632 - $15.00 USD Received 7 May 2013; revised 21 Jun 2013; accepted 2 Jul 2013; published 30 Aug 2013

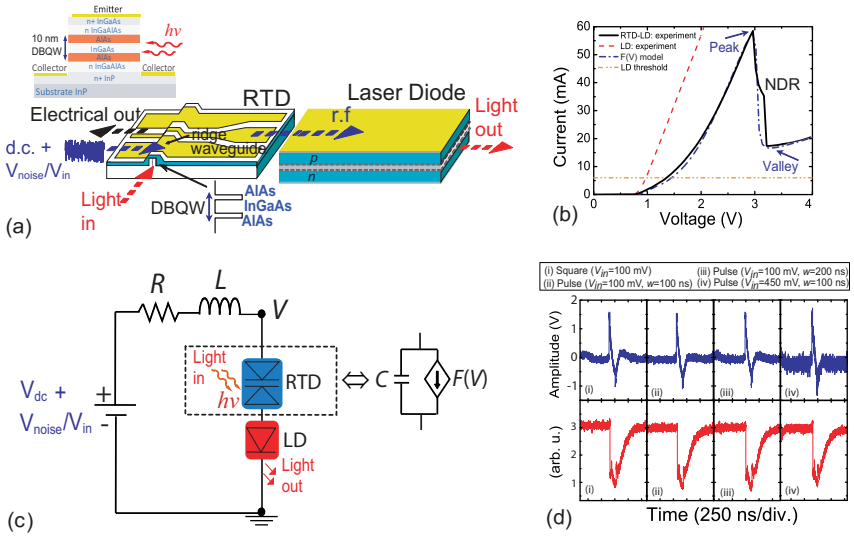

Fig. 1. (a) Schematic of the RTD photodetector and LD semiconductor chips forming the RTD-LD excitable optoelectronic device. Inset is the cross-section showing the epi-layer structure of the RTD. (b) Experimental I-V characteristics of LD, RTD-LD, and I-V model fit. (c) Equivalent electrical model of the RTD-LD circuit. (d) Excitable pulses in both the electrical and the optical RTD-LD outputs triggered by either a square or a pulse input signals at V_{dc} =2.9 V.

3. Theoretical model

The simplest model corresponding our optoelectronic circuit consist of single mode laser rate equations describing the photon and carrier number (S,N) of the LD dynamics coupled to the Liénard equations that governs the current and voltage in the RTD-LD (I,V):

$$\dot{V} = \frac{1}{\mu}\left[I - f(V) - \chi\xi(t)\right], \tag{1}$$

$$\dot{I} = \mu\left[V_{dc} + V_{in} - \gamma I - V\right] \tag{2}$$

$$\dot{N} = \frac{1}{\tau_n}\left[\frac{I}{I_{th}} - N - \frac{N-\delta}{1-\delta}\{1-\varepsilon S\}S\right] \tag{3}$$

$$\dot{S} = \frac{1}{\tau_p}\left[\frac{N-\delta}{1-\delta}\{1-\varepsilon S\}S - S + \beta N\right] \tag{4}$$

The dynamical system (1)-(4) has been successfully used to describe relaxation oscillations in RTD-LD devices [10]. The source of the RTD-LD oscillations is given by the NDR region of the nonlinear I-V characteristic function where $f(V)$ comes from the normalization of $F(V)$, represented by the function [13]:

$$f(V) = A\ln\left[\frac{1+e^{q(B-C+n_1V)/k_BT}}{1+e^{q(B-C-n_1V)/k_BT}}\right]\left[\frac{\pi}{2} + \tan^{-1}\left(\frac{C-n_1V}{D}\right)\right] + H\left(e^{n_2qV/k_BT} - 1\right) \tag{5}$$

In order to fit the model with the experimental I-V shown in Fig. 1(b) we use the fitting parameters: $A = 3.944\times10^{-3}$, $B = 0.109$, $C = 0.202$, $D = 2.08\times10^{-3}$, $H = 0.24$, $n_1 = 9.47\times10^{-2}$,

#189632 - $15.00 USD Received 7 May 2013; revised 21 Jun 2013; accepted 2 Jul 2013; published 30 Aug 2013

and $n_2 = 6.5 \times 10^{-4}$, and assume a voltage drop, $V_{th} \cong 0.84V$, to account to the LD voltage threshold. The parameters q and k_B are the electric charge and the Boltzmann constant, respectively.

In Eqs. (1)-(2) the parameters $\mu = V_0/I_0\sqrt{C/L}$ and $\gamma = R(I_0/V_0)$ are dimensionless parameters from the *LCR* circuit parameters, Fig. 1(c). The charge carrier N in Eqs. (3)-(4) is normalized to threshold providing that $\delta = N_0/N_{th}$, where N_0 is the carrier density for transparency, and N_{th} is the threshold carrier density; I_{th} is the laser threshold current parameter; ε stands for the dimensionless laser gain saturation, and β is the spontaneous emission contribution. The parameters τ_n and τ_p come from the time rescaling, where time is normalized to the characteristic *LC* resonant tank frequency, $\omega_0 = (\sqrt{LC})^{-1}$, hence $\tau = \omega_0 t$. Note that τ is redefined as as t in the final set of Eqs. (1)-(4). At last, we model the stochastic effects on the circuit dynamics behavior as an effective delta-correlated Gaussian white noise of zero mean $\chi\xi(t)$, where χ stands for the dimensionless variance of the distribution.

4. Results

The characteristics of a circuit with $L \sim 3$ μH are shown in Fig. 1(c). A region of NDR occurs for 2.95 V $\leq V_{dc} \leq$ 3.2 V. The circuit works in stationary regime for d.c. biases outside this interval while exhibits oscillatory behavior otherwise. When the RTD is biased in the first positive differential resistance region (PDR) slightly below the peak, it responds to weak external perturbations by emitting excitable pulses in both electrical and optical outputs when the perturbation exceeds a given threshold. We observed spiking behavior with identical shape and intensity triggered by either a square input signal or a train of pulses with amplitude levels, V_{in}, ranging from 100 mV to 450 mV, and pulse widths, w, from 100 ns to 200 ns, Fig. 1(d). The period of the injected signals was kept well above the lethargic time value. The time traces of Fig. 1(d)(top) show upward electrical spikes of identical shape with typical full width half maximum (FWHM) values of 13 ns triggered due to RTD-LD transitions from the peak-to-valley regions. The downward electrical pulses correspond to the valley-to-peak transitions before the RTD-LD system returns to its quiescent point. The LD intensity output, Fig. 1(d) (bottom), follows the electrical current switching induced by the RTD-LD with a sequence of downward pulses of identical shape and typical FWHM of $\sim$ 200 ns. If operated in the second PDR region, the direction of the electro-optical pulses would be reversed. We verified the existence of a critical threshold below which there is no response. The estimated critical value of the perturbation is 9 V.ns when d.c. biased at 2.9 V, e.g. a 100 ns square whose plateau is 90 mV.

Emission of excitable pulses can also be induced by electrical noise, Fig. 2. The upward electrical pulses have a typical FWHM of 13.5 ns [inset of (i)] with an identical shape as already shown in Fig. 1(d). Similarly, the LD intensity output, (ii), exhibits the identical response depicted in Fig. 1(d) with a typical FWHM of 201 ns [inset of (ii)]. While for low noise intensity these excitations are rare events, for higher noise strengths the RTD-LD fires more easily (iii) and (iv), with a time repetition getting closer to the RTD-LD's refractory time. In order to evaluate the typical lethargic time and the pulse statistics, we analyzed the interspike interval (ISI). Figures 2(b) and (c) present the histogram plots with a statistic of the times between minima of the laser output computed with a bin size of 20 ns as a function of noise strength. The d.c. bias voltage was used as a control parameter. The corresponding ISI distributions in Fig. 2(b) and (c) show the typical exponential behavior of a Kramer's escape process [7], displaced by the refractory time of the excitable orbits. Such a statistic with a hard boundary on the left allow us to estimate the refractory time to be around 500 ns ($\pm$ 20 ns). From the comparison between Figs. 2(b) and (c) we observe that the slope of the tail of the distribution decreases with increasing noise. In addition, as we increase the bias voltage less input noise intensity is required to obtain similar ISI distributions since increasing the bias voltage allows to approach the folding point

#189632 - $15.00 USD Received 7 May 2013; revised 21 Jun 2013; accepted 2 Jul 2013; published 30 Aug 2013

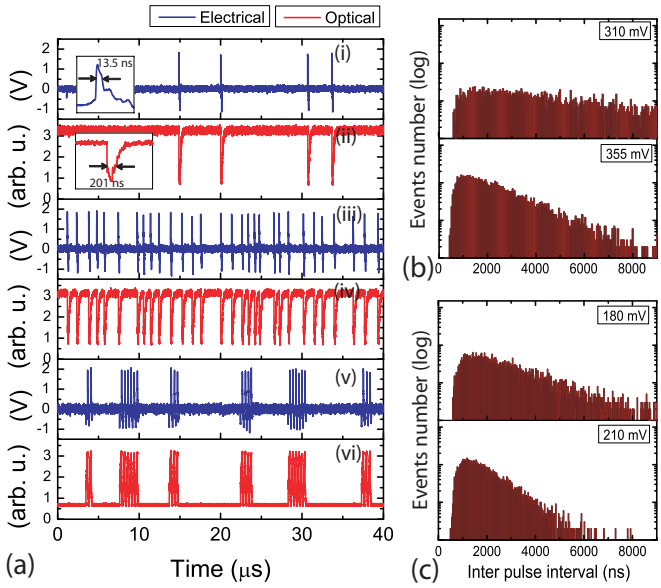

Fig. 2. (a) Experimental time traces of electrically noise induced neuron-like pulsing behavior in an RTD-LD excitable optoelectronic system in both the electrical and the optical domains. The RTD-LD is biased in the first PDR region (V_{dc}=2.9 V) and modulated with noise strength of (i)-(ii) 100 mV; (iii)-(iv) 175 mV. Multi-pulsing bursts when the RTD-LD is biased in the second PDR region, V_{dc}=3.2 V, and modulated with noise strength of 150 mV (v)-(vi). Histogram of the ISI statistics of the laser output as a function of noise amplitude and using the d.c. bias as a control parameter: (b) $V_{dc} = 2.85$ V; (c) $V_{dc} = 2.9$ V.

of the NDR which lower the excitable threshold and allows tuning the noise sensitivity.

Interestingly, the strongly asymmetric RTD-LD I-V characteristic, Fig 1(b), gives rise to two very different excitable regimes. In the first PDR the response consists in a single isolated peak while in the second PDR the temporal response is composed by a succession of peaks well separated by the lethargic time. Figures 2(a) (v) and (vi) shows multi-pulsing "bursting" behavior when the RTD-LD is d.c. biased in the second PDR region. Since the number of spikes can be controlled, at least partially, by tuning the distance from the oscillation threshold, this enrichs the dynamics and allows for some control of the excitable wave response. Such a feature would be either absent or limited to a small parameter vicinity in the case of excitable systems with a symmetric nullcline (e.g. Fitzhugh-Nagumo neuron model system).

The above observations can be fully explained with the model, Eqs. (1)-(4). The dimensionless parameters are chosen similarly as in [10] such as $\mu = 1.22 \times 10^{-3}$, $\gamma = 1.0$, $\tau_n = 1.22$, $\tau_p = 3061.8$, $\delta = 0.613$, $\varepsilon = 1.72 \times 10^{-3}$, and $\beta = 4 \times 10^{-4}$. We have analyzed the temporal traces, Fig. 3(a), using the same experimental conditions reported in Fig. 2. There is a very good agreement between the numerical simulation and the experimental results. The external noise added in the system is indeed responsible for randomly triggered pulses above the excitable threshold, and the ISI statistics, Figs. 3(b) and (c), present the same shape as observed in the experimental data. The multiple bursting in the second PDR is also reproduced by the asymmetry of the numerical $f(V)$ function. Although the increased clustering of the spikes is less pronounced than the experimental ones, modeling work that is currently underway suggests that simple refinements of the model, e.g., by considering the RTD capacitance dependence on the bias voltage, can provide a better agreement with experimental data.

#189632 - $15.00 USD Received 7 May 2013; revised 21 Jun 2013; accepted 2 Jul 2013; published 30 Aug 2013

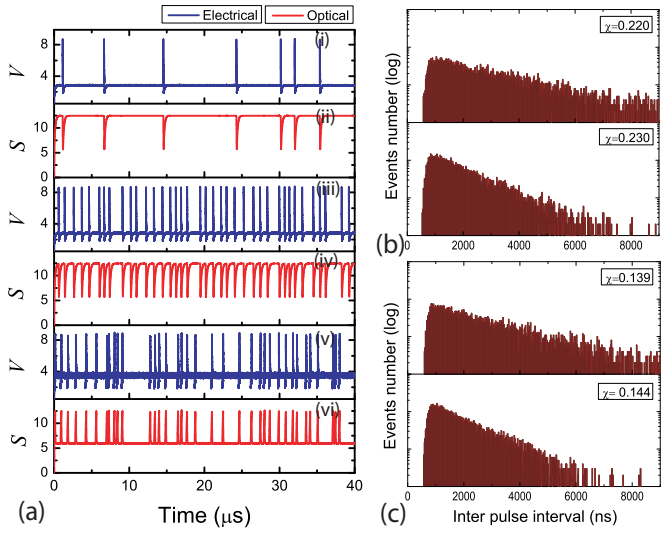

Fig. 3. (a) Numerical simulation of voltage and photon density, (V,S) showing noise induced pulsing dynamical regimes (i)-(iv) in the first PDR ($V_{dc} = 2.9$), and (v)-(vi) in the second PDR ($V_{dc} = 3.5$). The dimensionless noise strength employed in the simulations are: (i)-(ii) $\chi = 0.128$; (iii)-(iv) $\chi = 0.158$; and (v)-(vi) $\chi = 0.310$. ISI statistics of the laser output as a function of noise strength χ and using the bias voltage as a control parameter: (b) $V_{dc} = 2.85$; (c) $V_{dc} = 2.9$.

Our theoretical model explains in a simple way why the optical pulses seem broader than the voltage spikes. We note that the LD output is sensitive to the current provided by the RTD, and noticeable changes in intensity occur only during the slow stages of the excitable orbit. As shown schematically in Fig. 4, due to the asymmetric shape of the function $f(V)$, the large voltage jump that occurs in the first fast stage acts as an external driving force for I during the first slow stage. Instead, the second fast stage produces only a small voltage jump, which implies that during the second slow stage the RTD voltage is almost at its stationary value, i.e., $V \approx V_{dc} + V_{in}$, thus no external driving of I occurs. As a consequence, the voltage waveform is dominated by the first fast and slow stages, while the optical signal exhibits both slow stages, the latter lasting longer than the former.

With the help of the theoretical modeling results we can also obtain additional insight into the physical origin of the lethargic time of our excitable system. For the values of the parameters considered here ($\mu \ll 1$), we are clearly in presence of a slow-fast system, where the motion consists in the interchange of a fast motion and a slow motion along the nullclines defined by the $f(V)$ function, i.e. the two PDR regions, as discussed in Fig. 4. In the limit $\mu \ll 1$, the two fast stages can be neglected and the lethargic time corresponds mainly to the evolution along the slow stages defined by the two PDR regions. In these PDR regions, motion is governed by the equation $dI/d(\mu t) = V_{dc} - \gamma I - f^{-1}(I)$, that follows from the adiabatic elimination of Vusing that $\mu^{-1} \gg 1$. Since $f^{-1} \gg \gamma$, the period of the excitable orbit is proportional to $1/\mu = \sqrt{L/C}$ and to the derivative of f. Once the scaling of our model by $\omega_0 = (\sqrt{LC})^{-1}$ is removed, the lethargic time is solely proportional to the inductance of the circuit L. An approximate expression of the excitable period T_e can be estimated to be:

$$T_e/L = \frac{1}{f_2^{-1}} \ln \frac{V_{dc} - f_2^{-1} I_+}{V_{dc} - f_2^{-1} I_-} + \frac{1}{f_1^{-1}} \ln \frac{V_{dc} - f_1^{-1} I_-}{V_{dc} - f_1^{-1} I_+} \tag{6}$$

#189632 - $15.00 USD Received 7 May 2013; revised 21 Jun 2013; accepted 2 Jul 2013; published 30 Aug 2013

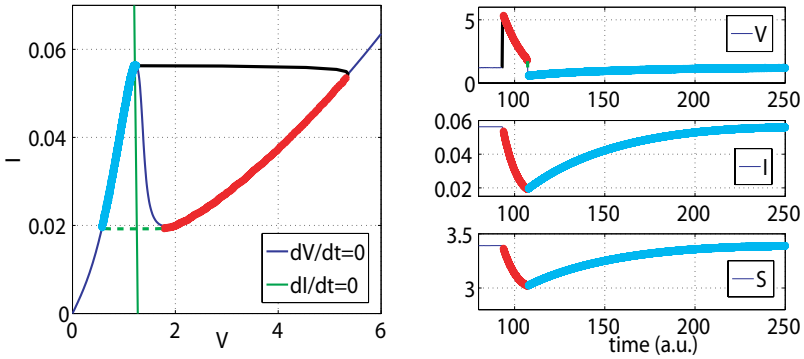

Fig. 4. Decomposition of the excitable orbit into four stages. The first fast stage corresponds to a sudden rise of the voltage (black line) without variation of the current. The second stage consists in a slow decay of both V and I along the right part of the $f(V)$ nullcline (red line). Next, another fast stage correspond to a voltage drop to the other side of the same nullcline (green dotted line) without variation of the current, finally followed by last slow stage where both V and I recover their initial values. The laser output being sensitive to the bias current, only the slow stages drive its evolution. $V_{dc} = 1.27$, see text for the values of the other parameters.

with $I_{\pm}$ the currents values at the folding points and $f_{1,2}^{-1}$ the inverse of the derivative of f in the first and second PDRs. Therefore, excitability and pulsating behavior can be achieved at faster speeds as a result of simple modifications of our optoelectronic circuit. Using a transmission line with $L \sim 8$ nH to connect the RTD and the LD dies and shunting the ensemble with a 10 Ω resistor connected physically close and in parallel to the RTD-LD, similarly to the high-frequency stabilization technique employed in circuits operating as oscillators at GHz frequencies [10], the pulse duration and lethargic time can be substantially reduced. Figures 5(a) and 5(b) show downward and upward optical pulses, respectively, triggered by a stochastic signal similarly to the lower speed circuit. We show in the inset of Fig. 5(b) a zoom of single pulse events in both the electrical and the optical outputs. The optical pulse exhibits a FWHM of 5.4 ns, and the upward voltage pulse event shows a FWHM of around 0.46 ns limited in part by the 100 ps time sampling.

Note that in Fig. 5(b) excitation events are triggered optically by taking advantage of the optical input port of the RTD ridge waveguide, Fig. 1(a), exhibiting a typical responsivity of around 0.25 A/W when DC biased in the second PDR region. In this experiment an optical signal at 1550 nm was amplitude modulated (AM) with electrical noise with sufficient modulation depth and optical power to trigger identical excitable orbits as observed in the electrical injection experiment. Although in terms of excitable response the optical injection method is not superior to the electrical injection one, which depends solely of the optoelectronic circuit characteristics, the results obtained show this system is a versatile excitable circuit controlled either by electrical or optical signals operating at telecommunication wavelengths.

Figure 5(c) and (d) presents the ISI statistic analysis of the time series found in the first and second PDRs. We find a statistic with a hard boundary on the left allowing to estimate the refractory time to be 12 ns ($\pm$ 500 ps) in the first PDR region, Fig. 5(c), and 9 ns ($\pm$ 500 ps) in the second PDR region, Fig. 5(d). The lethargic time is one order of magnitude lower than the one measured with the previous circuit. Further reduction would be expected with simple improvements either by reducing the RTD active area, or by reducing the series equivalent inductance, mainly determined by the length of the gold wires used in the connections.

#189632 - $15.00 USD Received 7 May 2013; revised 21 Jun 2013; accepted 2 Jul 2013; published 30 Aug 2013

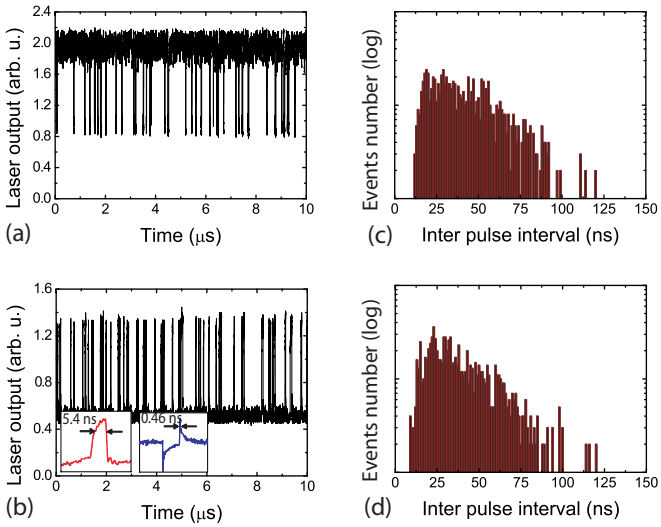

Fig. 5. Experimental photo-detected laser output time traces of: (a) electrically noise induced pulsing in the first PDR using a noise amplitude level of 600 mV; (b) optically induced pulsing in the second PDR employing a 5.5 mW optical power signal at $\lambda = 1550$ nm AM modulated with an electrical noise signal with 1.5 V amplitude. Inset: zoom of optical and electrical single pulses. Statistic of the times between minima/maxima in the laser output (with histogram bin size of 500 ps) when the RTD-LD is biased: (c) in the first PDR region ($V_{dc} = 2.0$ V), and (d) second PDR region ($V_{dc} = 2.075$ V).

5. Conclusion

In summary, we have demonstrated experimentally and numerically excitability and pulse generation in an original, simple and compact externally driven resonant tunneling-laser diode optoelectronic integrated circuit operating at telecommunication wavelengths. The excitable response is defined by lethargic times and pulse widths below 10 ns and 0.5 ns, respectively, obtained in both the electrical and the optical domains. Our optoelectronic system possesses the inherent capabilities for being used in the framework of bio-inspired data processing: a high potential for integrability, an intrinsic high speed response and quadruple electronic and optical inputs/outputs. Furthermore, since the current-voltage N-shape of RTD-LD is maintained almost from DC up to GHz frequencies, RTD-LD based excitable systems can be easily tuned for either low or fast speed excitable response depending of the desired application. Potential uses of our excitable system include ultra-fast neuro-inspired data processing, similar to reservoir computing, switching in optical networks, but also neural emulation applications such as associative memory or CNN-type computing architecture to perform complex information processing in neural inspired photonics networks.

Acknowledgments

This work was supported by FCT under the project WOWi (PTDC/EEA-TEL/100755/2008). B.R. thanks FCT Portugal for a Postdoctoral Fellowship (Grant No. SFRH/BPD/84466/2012). J.J. acknowledges financial support from the Ramon y Cajal fellowship. S.B., J.J. and O.P. acknowledge financial support from project RANGER (TEC2012-38864-C03-01 and from the Direcci General de Recerca del Govern de les Illes Balears co-funded by the EU FEDER funds. O. P. also acknowledges Grant FIS2010-22322-C02-01 (DAVID) from Ministry of Economics

and Competitivity of Spain.

#189632 - $15.00 USD Received 7 May 2013; revised 21 Jun 2013; accepted 2 Jul 2013; published 30 Aug 2013